Plastic collapse load of crown-hinged steel circular arches : a theoretical method

Plastic Collapse Load of Crown-Hinged Steel Circular Arches: A Theoretical Method

R.C. Spoorenberg*, H.H. Snijder and J.C.D. Hoenderkamp

Eindhoven University of Technology, Faculty of the Built Environment, The Netherlands

(Received: 6 December 2011; Received revised form: 14 June 2012; Accepted: 20 November 2012)

Abstract: For construction purposes and to avoid detrimental influences of foundation settlements arches are not always made from a single arch-rib but are built by connecting two curvilinear elements at the crown with a hinge. These arches are also known as crown-hinged arches. This paper presents an analytical procedure to approximate the plastic collapse load of circular crown-hinged steel arches. The development of the analytical method employs the lower- and upper bound theorem of plastic theory and the kinematic admissibility requirements. The influence of normal forces on the plastic moment capacity of the steel section is taken into account. The plastic collapse load is obtained by an iterative method as there is a non-linear relationship between the acting loads and the reduction of the plastic moment capacity due to normal forces. Through a comparison with earlier studies and finite element analyses, it is concluded that the proposed iterative method gives good results.

Key words: steel crown-hinged arch, plastic collapse load, yield contour, kinematic admissibility, iterative method, plastic theory.

1. INTRODUCTION

In many cases arches are built by joining two separate curvilinear segments together at the crown, thereby reducing the arch size to meet transport requirements and to create a statically determinate structure which is insensitive to detrimental effects of foundation settlements. The joint location is often significantly weaker compared to the arch-rib, and therefore idealized as a hinge. This crown hinge is able to transfer shear forces and normal forces but is unable to resist bending moments, leading to free rotation of the arch segments about the hinge axis. The introduction of a hinge at the crown in an arch without a crown hinge or so-called "continuous" arch [Figure 1(a)] reduces it to a crown-hinged arch [Figure 1(b)] and this will affect its structural response to loading. The stiffness and strength capacity of the arch will be reduced with the introduction of a hinge at the crown. Provided the arch has sufficient resistance to in-plane buckling [Figure 1(c)] and out-of-plane buckling [Figure 1(d)], the failure load of a crown-hinged arch can be approximated by the plastic collapse load [Figure 1(e)]. The in-plane elastic buckling behavior of one-hinged and three-hinged arches received large attention by Timoshenko and Gere (1961). Equations for elastic buckling loads were presented for parabolic arches under a vertical uniformly distributed load and circular arches subject to radially uniformly distributed loads, causing uniform compression in the arch-rib prior to buckling. The influence of bridge-deck stiffness on the in-plane buckling of three-hinged arches as applied in bridge-design was published by Hayashi (1971).

To the knowledge of the authors the only investigation into the plastic collapse load of crown-hinged arches was published by Yamasaki and Ishikawa (1968). They used differential equations to determine the elastic-plastic response of crown-hinged arches from the onset of loading up to plastic collapse. In addition

*Corresponding author. Email address: r.c.spoorenberg@tue.nl; Fax: +31-40-245-0328; Tel: +31-40-247-2948.

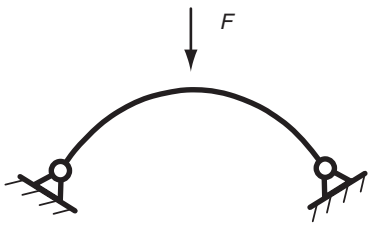

(a) "Continuous" arch

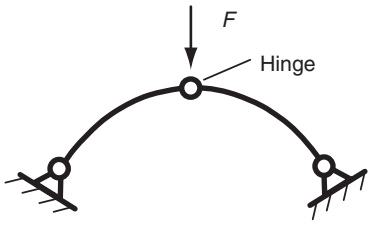

(b) Crown-hinged arch

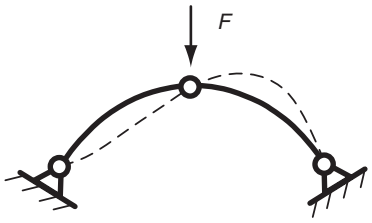

(c) In-plane instability

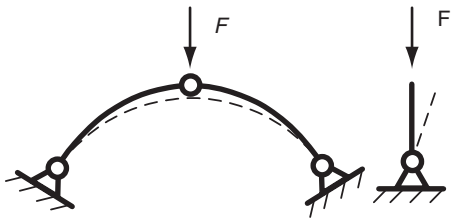

(d) Out-of-plane instability

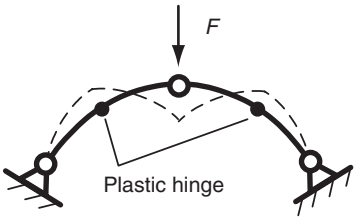

(e) In-plane plastic capacity

Figure 1. Arch lay-out, instability and plastic collapse load

limit load analyses were conducted. It was found that the introduction of a crown hinge in the arch reduces the plastic collapse load significantly. The study was

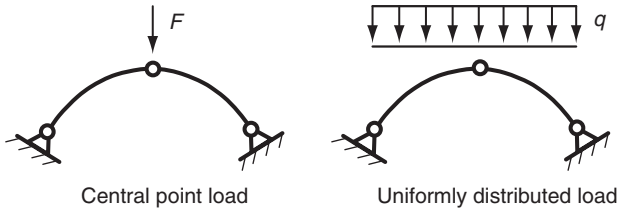

(a) Three-hinged arch

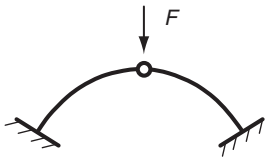

Central point load

(b) One-hinged arch

Figure 2. Load cases and support conditions investigated

confined to pin-supported arches made from I-sections, for which a simplified yield contour was used. Expanding these limit analyses to include crown-hinged arches with other yield contours and support conditions would require a significant extension of their work.

In this paper, a different approach to study the plastic collapse of crown-hinged circular steel I-section arches is presented. An analytical approach is used, which is applicable to a wide range of arch geometries and cross-sections. It allows a change in the structural parameters without changing the underlying equilibrium equations. Pin-supported circular arches with a hinge at the crown subjected to either a central point load or a uniformly distributed load are analyzed [Figure 2(a)] in addition to fixed circular arches with a hinge at the crown subjected to a central point load [Figure 2(b)]. Pin-supported arches with a hinge at the crown and fixed arches with a hinge at the crown are referred to as three-hinged and one-hinged arches respectively, throughout this paper. All arches have a constant cross-section along the developed arch-length.

2. METHODOLOGY FOR PLASTIC COLLAPSE ANALYSIS

Plastic collapse analyses are frequently used to obtain the plastic collapse load of beams and frames, whereby a lower bound theorem or an upper bound theorem is used. In the present study, both theorems are combined. As part of the lower bound theorem, a bending moment distribution and normal force distribution are assumed in the arch-rib that are in equilibrium with the external loads and for which the yield criterion is not violated. A mechanism condition

is assumed with a sufficient number of plastic hinges, which reduces the arch to a plastic collapse mechanism as part of the upper bound theorem. Both theorems are combined by adjusting the bending moment and normal force distributions such that they satisfy the mechanism condition, without violating the yield contour. This yields an exact value for the plastic collapse load. The deformation mode must be checked to be in agreement with the kinematic admissibility of the collapse mode.

2.1. Plastic Hinge Locations

A three-hinged and a one-hinged arch are statically determinate and statically indeterminate to the second degree, respectively. From a redundancy point of view a three-hinged arch has no redundancy and a one-hinged arch has two redundancies. Reducing a three-hinged arch to a mechanism requires the formation of one plastic hinge [Figure 3(a)] whereas three plastic hinges are necessary to form a plastic mechanism in a one-hinged arch [Figure 3(b)]. Possible plastic hinge locations are between the crown and the support or at the support. When an arch is loaded and supported symmetrically, plastic hinges can emerge simultaneously on both sides of the crown, rendering two plastic hinges in excess of the arch redundancy instead of one. The crown-hinge location is denoted by number "1". The plastic hinges are numbered according to their location on the arch-rib. The plastic hinge forming between the crown and the support is denoted by number "2". The plastic hinge forming at the support is denoted by number "3". The formation of two plastic hinges in a three-hinged arch [Figure 3(c)] or four plastic hinges in a one-hinged arch [Figure 3(d)] can take place when the arch is mostly subject to bending. In this case it fails by a so-called flexural mechanism, e.g. for arches with a large rise-to-span ratio (*f/L*) [Figure 3(e)]. However, for shallow arches with small rise-to-span ratios, compressive action is predominant, causing the arch to fail by a so-called compressive mechanism, Bakker *et al.* (2008) [Figure 3(f)]. By examining the kinematic admissibility of the collapse mode it can be checked whether the correct mechanism has been selected.

2.2. Assumptions

The proposed analyses are based on 1st order plastic theory: equilibrium is defined in the undeformed shape of the arch. The moment-curvature relationship of the cross-section is assumed to be rigid plastic, which is a simplification of the true moment-curvature behavior [Figure 4(a)]. Hence it is assumed that no deformations take place prior to the attainment of the plastic collapse load. The cross-section of the arch is able to sustain sufficient rotations under plastic moment without failing by local buckling, allowing redistribution of forces in the arch-rib during the course of loading. Only sections belonging to class 1 according to Eurocode 3 EN 1993-1-1 (2004) will therefore suffice. The influence of shear force on the plastic moment capacity and normal force capacity is not taken into account. Sagging moments and hogging moments are denoted as positive and negative, respectively. Compressive forces are taken as negative and tensile forces are taken as positive.

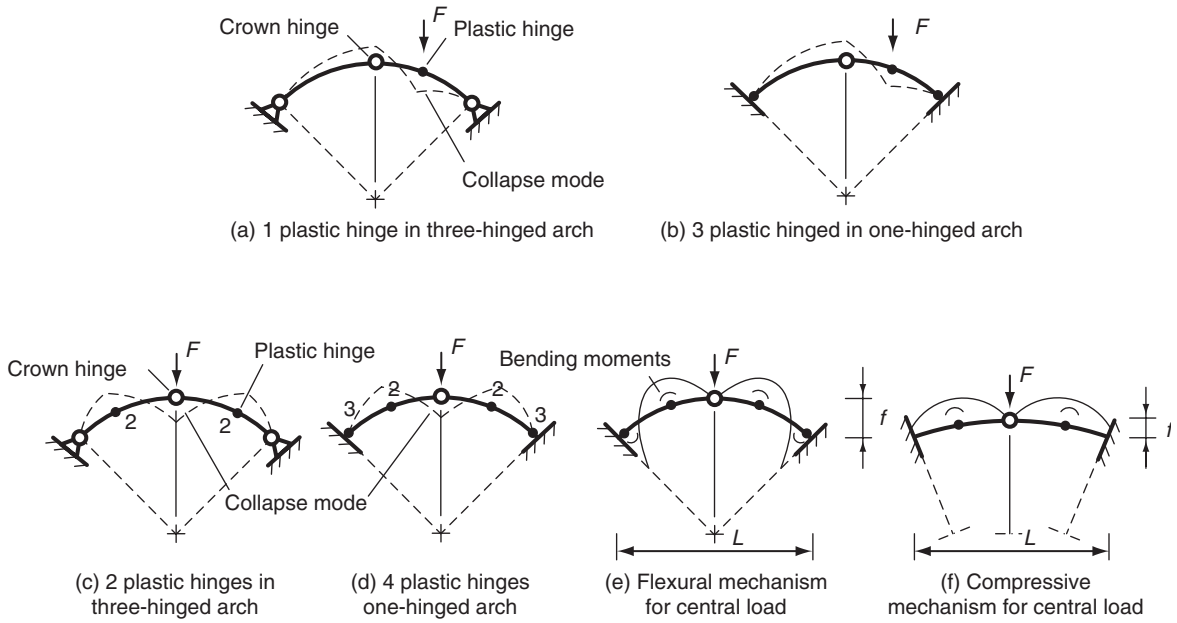

Figure 3. Arch configurations, collapse mechanisms and possible hinge locations

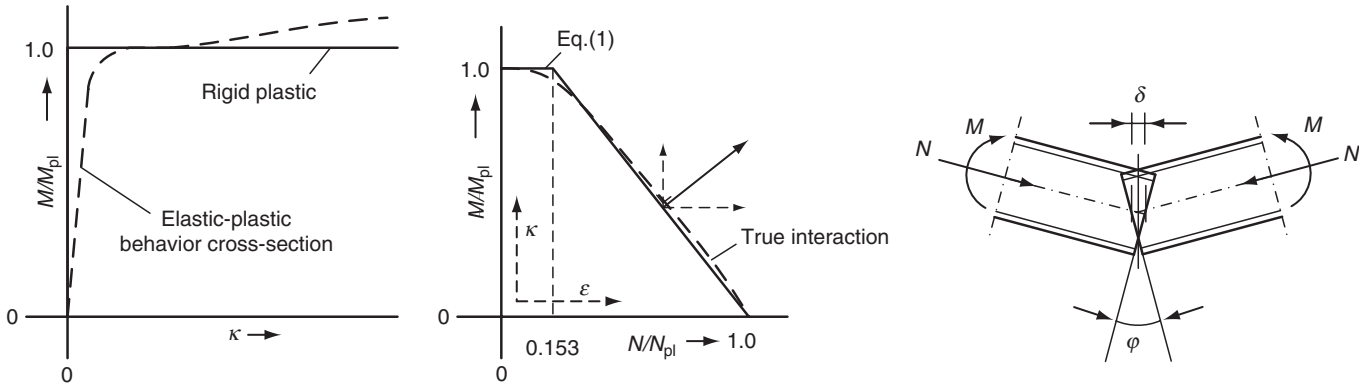

Figure 4. Moment-normal force interaction

2.3. Yield Contour and Normality Rule

The yield contour quantifies the influence of the normal force on the plastic moment capacity of a steel section. Depending on the shape of the cross-section, many yield contours are available in the literature to approximate the moment-normal force relationship. The present study is confined to wide flange sections bent about their major axis for which the yield contour ψ is as follows:

$$\psi = \left|\frac{M}{M_{\text{pl}}}\right| - 1.0 = 0 \quad \text{for } 0 \le \left|\frac{N}{N_{\text{pl}}}\right| \le 0.153$$

$$\psi = 1.18\left(1.0 - \left|\frac{N}{N_{\text{pl}}}\right|\right) - \left|\frac{M}{M_{\text{pl}}}\right| = 0 \qquad (1)$$

$$\text{for } 0.153 \le \left|\frac{N}{N_{\text{pl}}}\right| \le 1.0$$

In which M_{pl} is the full plastic moment, M is the bending moment, N_{pl} is the squash load of the cross section and N is the axial force. This yield contour is a generally accepted engineering approximation of the true curve [Figure 4(b)] and has seen widespread application in the design of steel structures: Trahair *et al.* (1997) and Trahair *et al.* (2007). As the yield contour is symmetric with respect to the coordinate axes, only one quadrant is shown. The normality rule relates the finite rotation (φ), contraction (δ), curvature (κ) and axial strain (ε) to each other for any combination of moment and normal force.

$$\frac{dM}{dN} = -\frac{\partial\psi/\partial N}{\partial\psi/\partial M} = -\frac{\varepsilon}{\kappa} = \pm\frac{1.18M_{\text{pl}}}{N_{\text{pl}}} = \pm\frac{\delta}{\varphi}$$

$$\text{for} \quad 0.153 \le \left|\frac{N}{N_{\text{pl}}}\right| \le 1 \qquad (2)$$

$$\frac{dM}{dN} = 0 \quad \text{for} \quad 0 \le \left|\frac{N}{N_{\text{pl}}}\right| \le 0.153 \qquad (3)$$

The lower sign corresponds to the case where the moments and normal forces have opposite sign (e.g. sagging moments and compressive forces). The upper sign corresponds to the case where the bending moments and normal force in the plastic hinge have the same sign (e.g hogging moment and compressive force).

3. ANALYSES

3.1. Three-Hinged Arch with Central Point Load

The symmetric conditions of a three-hinged arch with a central point load allow the investigation to be performed on only a half arch. The half arch geometry is expressed by the subtended angle γ and the arch radius R. The angular coordinate system θ is used to describe the normal force distribution, bending moment distribution and plastic hinge location, for which: $0 \le \theta \le \gamma$. The crown hinge is located at the angle: $\theta_1 = \theta = 0$. This hinge is annotated as no. 1. The plastic hinge with reduced plastic moment capacity $M_{\text{pl2;red}}$ is located at an angle θ_2 in between crown and support. The reduction of the plastic moment capacity in the plastic hinges is according to Eqn 1.

The reaction forces depicted in Figure 5(a) can be computed by considering equilibrium:

$$R_{\text{BV}} = \tfrac{1}{2}F \quad R_{\text{AH}} = R_{\text{BH}} = \frac{\tfrac{1}{2}FR\sin\gamma}{R(1-\cos\gamma)} \qquad (4)$$

The reaction force at the support equals the compressive force at the crown, as no other horizontal forces act on the arch:

$$R_{\text{BH}} = N(\theta = 0) = -N_1 \qquad (5)$$

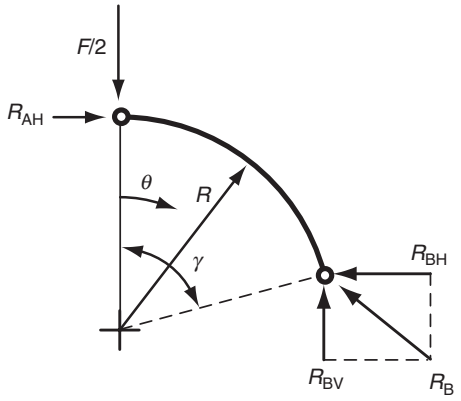

(a) Geometry and loading

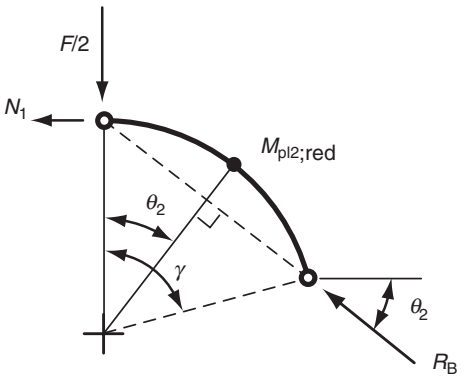

(b) Funicular line and plastic hinge

Figure 5. Half-arch of symmetric structure

By substituting Eqn 5 into Eqn 4 a first estimate of the plastic collapse load F_{est} can be obtained for any value of the normal force at the crown, N_1:

$$F_{\text{est}} = \frac{2N_1R(\cos\gamma - 1)}{R\sin\gamma} \tag{6}$$

The bending moment distribution at plastic collapse is given by the following equation:

$$M(\theta) = R_{\text{AH}}R(1-\cos\theta) - \tfrac{1}{2}FR\sin\theta \tag{7}$$

The normal force distribution can be presented as follows:

$$N(\theta) = -R_{\text{BH}}\cos\theta - R_{\text{BV}}\sin\theta \tag{8}$$

The plastic collapse load is found when the acting bending moment equals the reduced plastic moment capacity $M_{\text{pl2;red}}$ at angular coordinate $\theta = \theta_2$:

$$M(\theta_2) = -M_{\text{pl2;red}} \tag{9}$$

When combining Eqn 9 with 7 and 4 the plastic collapse load F (which is now referred to as F_{pl}) can be obtained as follows:

$$F_{\text{pl}} = \frac{2\left(M_{\text{pl2;red}} - M_{\text{pl2;red}}\cos\gamma + M_{\text{pl2;red}}\cos\theta_2\right)}{R\left(\sin(\gamma-\theta_2) - \sin\gamma + \sin\gamma/2\right)} \tag{10}$$

The angular coordinate of the second plastic hinge is found by setting $dF_{\text{pl}}/d\theta_2$ equal to zero and solving for θ_2 [Figure 5(b)]. This yields:

$$\theta_2 = \gamma/2 \tag{11}$$

The plastic hinge forms at the location of the maximum hogging moment. This location is where the distance between the funicular line and the arch-rib has the largest value. The compressive force at the second plastic hinge can be obtained by using the reaction forces [Figure 5(b)]:

$$N_2 = -R_{\text{B}} = -\sqrt{{R_{\text{BH}}}^2 + {R_{\text{BV}}}^2} \tag{12}$$

A first approximation for N_1 yields a first estimate of the plastic collapse load: $F_{\text{est}}(6)$. By substituting F_{est} into Eqn 4 and employing Eqn 12, the compressive force at plastic hinge no. 2, N_2, can be determined. Subsequently the reduced plastic moment capacity $M_{\text{pl2;red}}$ can be determined with the yield contour from section 2.3. Substituting Eqn 11 and $M_{\text{pl2;red}}$ into Eqn 10 yields the plastic collapse load F_{pl}. Two different plastic collapse loads are determined for each value of N_1: F_{est} and F_{pl}. The plastic collapse load is obtained if $F_{\text{est}} = F_{\text{pl}}$. A possible mismatch between F_{est} and F_{pl} is caused by an incorrect approximation of N_1 and requires the determination of a new normal force N_1 to restart the calculations. As the value of N_1 for which $F_{\text{est}} = F_{\text{pl}}$ is not known in advance, an iterative procedure is required. An improved estimate of N_1 can be obtained with the (iterative) bisection method. If N_1 is assumed too small, then $F_{\text{est}} > F_{\text{pl}}$. If N_1 is assumed too large, then $F_{\text{est}} < F_{\text{pl}}$. The iterations are stopped if the ratio $F_{\text{est}}/F_{\text{pl}}$ deviates from unity within a specified tolerance e. For all analyses in this study e was set at 0.001. The flow chart of the bisection method is shown in Figure 6. The reduced plastic moment of every cross-section must not be exceeded by the acting moments:

$$M(\theta) \le \left|M_{pl;red}(\theta)\right| \tag{13}$$

3.2. Three-Hinged Arch with Uniformly Distributed Load

By considering equilibrium of one half of the arch, the reaction forces at the support of a three-hinged arch with a uniformly distributed load are [Figure 7(a)]:

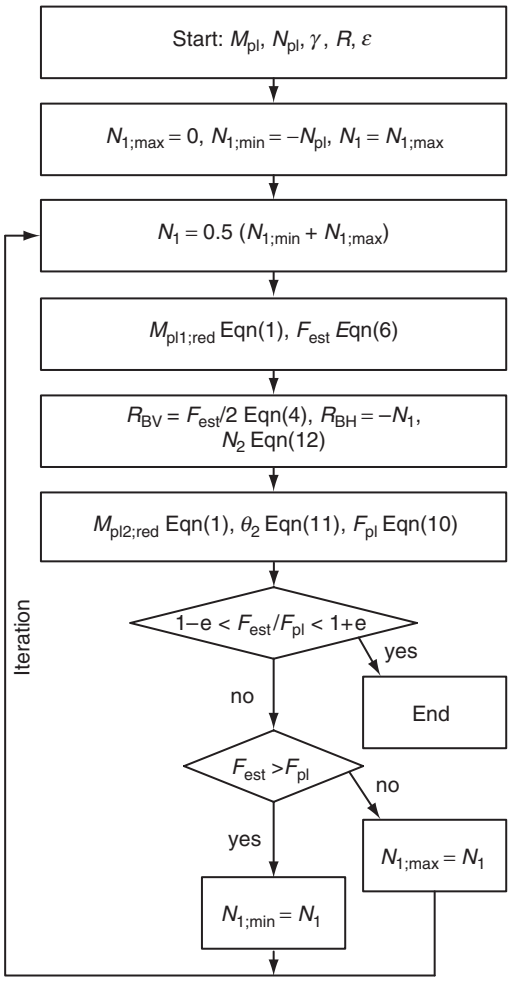

Figure 6. Flow chart of bisection method for a three-hinged arch with central point load

$$R_{BV} = qR\sin\gamma \quad R_{AH} = R_{BH} = \frac{\frac{1}{2}qR^2(\sin\gamma)^2}{R(1-\cos\gamma)} \tag{14}$$

The horizontal component of the reaction force at the support equals the compressive action at the crown (Eqn 5). By employing this equation, a first estimate of the plastic collapse load q_{est} can be made for any value of N_1:

$$q_{est} = \frac{2(-N_1R + N_1R\cos\gamma)}{R^2(\sin\gamma)^2} \tag{15}$$

The bending moment M and the axial compression force N along the arch can be calculated as follows:

$$M(\theta) = R_{BH}R(1-\cos\theta) - \tfrac{1}{2}qR^2\sin\theta \tag{16}$$

$$N(\theta) = -R_{BH}\cos\theta - qR(\sin\theta)^2 \tag{17}$$

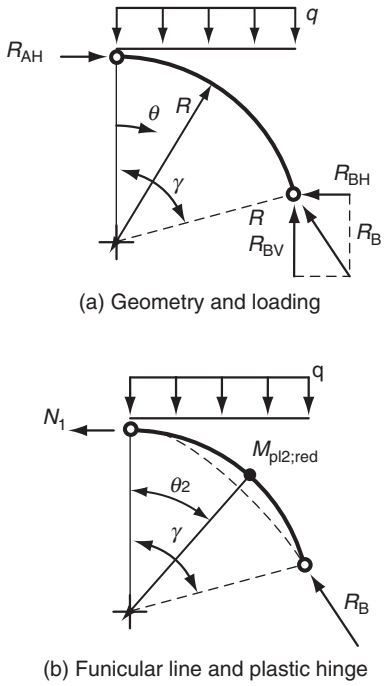

Figure 7. Half-arch of symmetric structure with a uniformly distributed load

Similarly to three-hinged arches with a central point load, plastic collapse for the three-hinged arch with a uniformly distributed load takes place when two plastic hinges are formed simultaneously on either side of the crown [Figure 7(b)]. The bending moment then equals the reduced plastic moment capacity: Eqn 9. Employing Eqns 14, 16 9 and solving for q (hereafter referred to as q_{pl}) results in an expression for the uniformly distributed plastic collapse load:

$$q_{pl} = \frac{M_{pl2;red}}{R^2(-\cos\gamma + \cos\theta_2)\sin(\theta_2/2)^2} \tag{18}$$

In which θ_2 is the angular coordinate of the plastic hinge between the crown and support. From Eqn 18 it can be seen that q_{pl} depends on the location of the plastic hinge. The absolute minimum value for q_{pl} is found by setting $dq_{pl}/d\theta_2 = 0$ and solving for θ_2 which is the angular coordinate of plastic hinge 2:

$$\theta_2 = 2arc\cot\sqrt{\frac{-3-\cos\gamma}{-1+\cos\gamma}} \tag{19}$$

The compressive force N_2 at this angle can be determined from the following equation:

$$N_2 = -\sqrt{(q_{est}R\sin\theta_2)^2 + R_{BH}{}^2} \tag{20}$$

Any value of N_1 will yield two different plastic collapse loads: q_{est} and q_{pl}. A first estimate for N_1 will produce a value of the plastic collapse load q_{est} using Eqn 15. Subsequently the reaction forces at the support, R_{BV} and R_{BH} are determined with Eqn 14, employing q_{est}. From the reaction forces the compressive force N_2 at plastic hinge 2 can be obtained with Eqn 20. Subsequently the reduced plastic moment capacity can be determined by employing N_2 in the yield contour according to Eqn 1. With θ_2 from Eqn 19 and the reduced plastic moment capacity $M_{pl2;red}$, the plastic collapse load q_{pl} can be obtained from Eqn 18. A mismatch between q_{est} and q_{pl} is caused by a crude estimate for N_1 and hence a new value for N_1 needs to be determined. An improved estimate of N_1 is made with the (iterative) bisection method (Figure 8). If N_1 is assumed too small, then $q_{est} > q_{pl}$. If N_1 is assumed too large, then $q_{est} < q_{pl}$. When the ratio q_{est}/q_{pl} is within the specified tolerance limit e the iterations are stopped. As a final check the plasticity condition given in Eqn 13 must be verified.

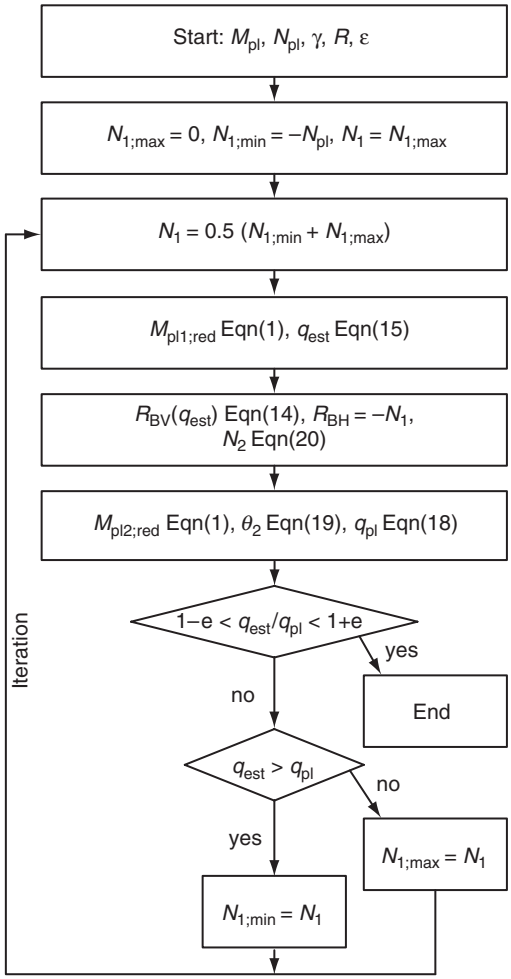

Figure 8. Flow chart of bisection method for a three-hinged arch with a uniformly distributed load

3.3. One-Hinged Arch with Central Point Load

For a one-hinged arch it is assumed that the first plastic hinge develops at the support. This hinge is replaced by a reacting moment $M_{pl3;red}$ which imposes a reactant moment distribution on the arch-rib. The one-hinged arch fails by a vertical mechanism [Figure 3(d)], i.e. the second plastic hinge develops simultaneously at angle θ_2 in the left and right parts of the arch. Thus, a total of four plastic hinges in the arch structure are formed.

The reaction forces at the supports can be determined by considering the free-body diagram [Figure 9(a)]:

$$R_{BV} = F/2 \quad R_{AH} = R_{BH} = \frac{\frac{1}{2}FR\sin\gamma + M_{pl3;red}}{R(1-\cos\gamma)} \quad (21)$$

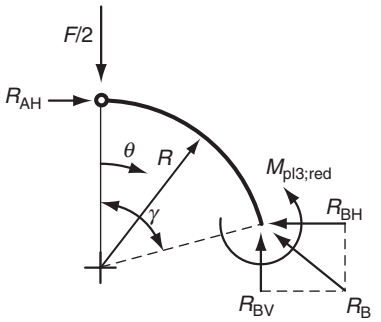

(a) Geometry and loading

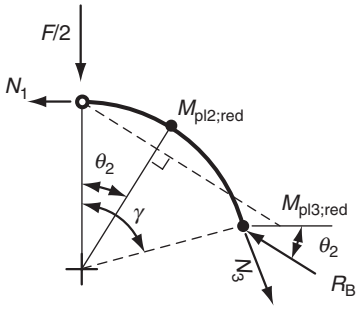

(b) Funicular line and plastic hinges

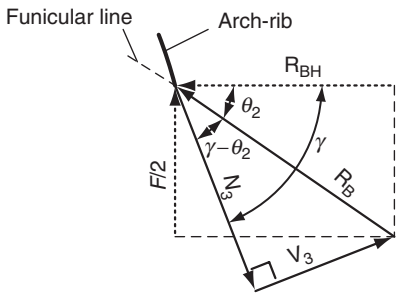

(c) Force composition at support

Figure 9. Half-arch geometry of symmetric structure and reaction force at support

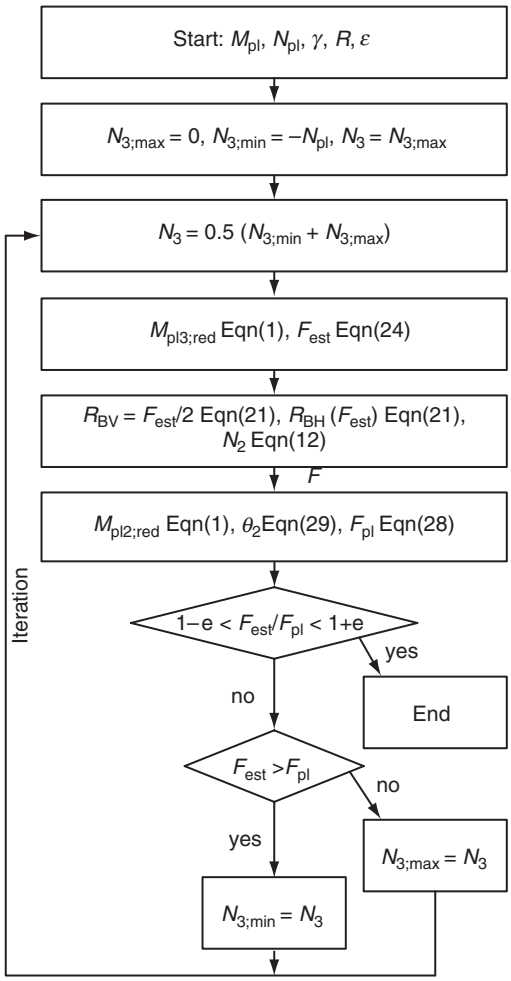

Figure 10. Flow chart of bisection method for a one-hinged arch with central point load

The angle at which the second plastic hinge is formed can be computed as follows [Figure 9(b)]:

$$\theta_2 = \arctan\left(F/2R_{BH}\right) \tag{22}$$

From this the compressive action at the support N_3 [Figure 9(c)] can be determined:

$$N_3 = -\cos\left(\gamma - \theta_2\right)\frac{F}{2\sin\theta_2} \tag{23}$$

In the previous analyses the compressive force at the crown, N_1, was selected as the pivotal variable in the derivation of subsequent equilibrium equations. However, for the one-hinged arch with a central point load N_1 is not feasible, and therefore recourse was taken to the compressive force at the support, N_3 to derive the equilibrium equations. Substituting Eqn 21 into Eqn 22 and combining with Eqn 23 gives an equation for the plastic collapse load F_{est} (replacing F) for a first estimate of N_3:

$$F_{est} = \frac{\begin{array}{c}-2\left(M_{pl3;red} + N_3 R\right) + \left(1/\sin\gamma\right) \\ \times\left(8\sqrt{{C_1}^2\cos\left(0.5\gamma\right)^2\,\mathrm{Sin}\left(0.5\gamma\right)^6} - C_1\sin 2\gamma\right)\end{array}}{2R\sin\gamma} \tag{24}$$

where:

$$C_1 = M_{pl3;red} - N_3 R \tag{25}$$

With N_3 the reduced plastic moment $M_{pl3;red}$ is obtained from the yield contour given in section 2.3. The bending moment distribution and compressive forces along the arch-rib are given by the following equations:

$$\begin{aligned} M\left(\theta\right) &= M_{pl3;red} - R_{BH}R\left(\cos\theta - \cos\gamma\right) \\ &\quad + \tfrac{1}{2}FR\left(\sin\gamma - \sin\theta\right) \end{aligned} \tag{26}$$

$$N\left(\theta\right) = -R_{BH}\cos\theta - R_{BV}\sin\theta \tag{27}$$

Utilizing Eqn 26 and Eqn 21 for substitution into Eqn 9 yields the plastic collapse load F (hereafter is referred to as F_{pl}) based on the plastic moment capacity $M_{pl2;red}$ and the angular coordinate of the second plastic hinge, θ_2:

$$F_{pl} = \frac{\begin{array}{c}2(M_{pl2;red} + M_{pl3;red} - M_{pl2;red} \\ \times\cos\gamma - M_{pl3;red}\cos\theta_2)\end{array}}{R\left(-\sin\gamma + \sin\left(\gamma - \theta_2\right) + \sin\theta_2\right)} \tag{28}$$

The angular coordinate of the second plastic hinge is found by setting $dF_{pl}/d\theta_2$ equal to zero and solving for θ_2:

$$\theta_2 = \mathrm{arc\,sec}\frac{\begin{array}{c}-\left(2{M_{pl2;red}}^2 - 2M_{pl2;red}M_{pl3;red} - {M_{pl3;red}}^2\right. \\ \left.+2M_{pl2;red}C_2\cos\gamma\right)\sin\left(0.5\gamma\right)^4 \\ +4\sqrt{{M_{pl2;red}}^3 C_2\cos\left(0.5\gamma\right)^2\sin\left(0.5\gamma\right)^{12}}\end{array}}{M_{pl3;red}\left(C_2 - M_{pl2;red}\cos\gamma\right)\sin\left(0.5\gamma\right)^4} \tag{29}$$

where:

$$C_2 = M_{pl2;red} + M_{pl3;red} \tag{30}$$

With a first approximation for N_3, the plastic collapse load F_{est} can be estimated with Eqn 24 and the reduced plastic moment at the support $M_{pl3;red}$ according to Eqn 1. With F_{est} the reaction forces R_{BH} and R_{BV} can be calculated using Eqn 21, which in turn are used to evaluate the compressive force at the second plastic hinge N_2 with Eqn 12. The reduced plastic moment

capacity $M_{pl2;red}$ can be obtained by substituting N_2 into the yield contour given by Eqn 1. Employing $M_{pl2;red}$ and $M_{pl3;red}$ gives the location of the second plastic hinge θ_2 with Eqn 29 which leads to F_{pl} from Eqn 28. Hence two different plastic collapse loads are obtained: F_{est} and F_{pl}. Any mismatch between these values is caused by an inaccurate estimate of N_3 and requires a new approximation. The plastic collapse load is found for a value of N_3 for which $F_{est} = F_{pl}$. The (iterative) bisection method is used to make an improved estimate N_3. If N_3 is assumed too small, then $F_{est} > F_{pl}$. If N_3 is assumed too large, then $F_{est} < F_{pl}$. When the ratio F_{est}/F_{pl} is within a specified tolerance value e the normal force at the onset of plastic collapse is obtained and the iterations are terminated. The reduced plastic moment capacity at every cross-section must not be exceeded by the applied bending moment. This can be verified by Eqn 13.

3.4. Kinematic Admissibility

The introduction of a sufficient number of plastic hinges in the arch-rib reduces the arch to a plastic collapse mechanism. In order to make sure that the prescribed mechanism will indeed develop and that the obtained plastic collapse load is physically meaningful, the collapse mode must meet the kinematic admissibility requirements. The rotations φ_i and contractions δ_i in plastic hinge i are shown in Figure 11, where subscript i denotes the number of the (plastic) hinge in accordance with the previous sections. As the material displays plastic yielding under constant force, the magnitude of the deformations cannot be determined but they are normalized with respect to φ_1.

In order for the prescribed mechanism to develop, the following kinematic admissibility requirements must be met:

$$\Delta_{ver}/\varphi_1 \geq 0 \tag{31}$$

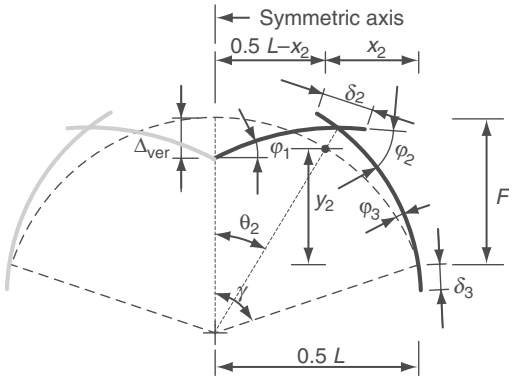

Figure 11. Collapse mechanism (deformations and rotations shown as positive)

$$\varphi_2/\varphi_1 \geq 0 \tag{32}$$

$$\varphi_3/\varphi_1 \geq 0 \tag{33}$$

The kinematic admissibility requirement given by Eqn 31 ensures that the crown moves in the same direction as the acting loads. Eqns 32 and 33 imply that negative (hogging) moments must take place at plastic hinge 2 and positive (sagging) moments at plastic hinge 3 in order for the flexural mechanism to develop. Eqn 33 applies to one-hinged arches only. The displacement of the crown can be described in terms of rigid body movement of the arch sections:

$$\Delta_{ver} = \left(\tfrac{1}{2}L - x_2\right)\varphi_2 - \tfrac{1}{2}L\varphi_3 + \delta_2 \sin\theta_2 + \delta_3 \sin\gamma \tag{34}$$

Where L is the horizontal span of the complete arch and x_2 the horizontal coordinate of plastic hinge no. 2. The following equations relate the span length L and horizontal coordinate x_2 of plastic hinge no. 2 to the subtended angle and arch radius:

$$L = 2R\sin\gamma \quad x_2 = \tfrac{1}{2}L - R\sin\theta_2 \tag{35}$$

The relationship between the contraction and rotation of each individual (plastic) hinge can be represented by the following equations:

$$-\frac{\varepsilon_1}{\kappa_1} = \frac{\delta_1}{\varphi_1} = c_1 \quad \frac{\varepsilon_2}{\kappa_2} = \frac{\delta_2}{\varphi_2} = c_2 \quad -\frac{\varepsilon_3}{\kappa_3} = \frac{\delta_3}{\varphi_3} = c_3 \tag{36}$$

The behavior of the crown hinge is featured by rotation φ_1 and absence of contraction, i.e. $\delta_1 = 0$, hence $c_1 = 0$. For three-hinged arches contraction does not take place at the support, hence $c_3 = 0$. The rotations are related by the following equation:

$$\varphi_3 = \varphi_2 - \varphi_1 \tag{37}$$

As the horizontal deformation at the crown Δ_{hor} is equal to zero, arch closure is also represented by the following equation:

$$\begin{aligned}\Delta_{hor} = f\varphi_3 - \left(f - y_2\right)\varphi_2 + \delta_1 + \delta_2\cos\theta_2 \\ + \delta_3\cos\gamma = 0\end{aligned} \tag{38}$$

Where f is the rise of the arch and y_2 the vertical position of plastic hinge no. 2, which can be obtained as follows:

$$f = R\left(1 - \cos\gamma\right) \quad y_2 = f - R\left(1 - \cos\theta_2\right) \tag{39}$$

When employing Eqns 36, 37, 38 and $c_1 = 0$, the kinematic admissibility requirement of Eqn 32 can be rewritten as follows:

$$\frac{\varphi_2}{\varphi_1} = \frac{f + c_3 \cos\gamma}{y_2 + c_2 \cos\theta_2 + c_3 \cos\gamma} \geq 0 \tag{40}$$

Eqn 33 can be rewritten by utilizing Eqns 37 and 40:

$$\frac{\varphi_3}{\varphi_1} = \frac{f - y_2 - c_2 \cos\theta_2}{y_2 + c_2 \cos\theta_2 + c_3 \cos\gamma} \geq 0 \tag{41}$$

By employing Eqns 34, 36 and 40 the kinematic admissibility requirement represented by Eqn 31 can be rewritten as:

$$\begin{aligned} &\frac{\Delta_{\text{ver}}}{\varphi_1} = \frac{f + c_3 \cos\gamma}{y_2 + c_2 \cos\theta_2 + c_3 \cos\gamma} \\ &\left(-x_2 + c_2 \sin\theta_2 + c_3 \sin\gamma\right) + \left(\tfrac{1}{2}L - c_3 \sin\gamma\right) \geq 0 \end{aligned} \tag{42}$$

The kinematic admissibility of the plastic collapse mode can be checked by applying Eqns 40 and 42 for three-hinged arches. For one-hinged arches Eqns 40, 41 and 42 must be employed. These kinematic admissibility requirements will be used later to check the validity of the calculated collapse loads.

4. COMPARISON WITH YAMASAKI AND ISHIKAWA

As part of a larger study on the elastic-plastic response of steel arches, Yamasaki and Ishikawa (1968) investigated three-hinged arches with a central point load and with a uniformly distributed load.

4.1. Yield Contour

The adopted yield contour was based on an idealization of a moment-normal force interaction for an I-section bent about its major axis. To describe this yield contour, the ratio between the sectional area of the flanges and the sectional area of the web was used:

$$\rho = \frac{A_{\text{f}}}{A_{\text{w}}} = \frac{2bt_{\text{f}}}{ht_{\text{w}}} \tag{43}$$

where:

A_{f} is the area of the flanges
A_{w} is the area of the web
h is the height of the cross-section
b is the flange width of the cross-section
t_{f} is the flange thickness
t_{w} is the web thickness

The elastic moment capacity is given by:

$$M_{\text{y}} = \left(1 + 3\rho\right) t_{\text{w}} h^2 f_{\text{y}} \big/ 6 = W_{\text{el}} f_{\text{y}} \tag{44}$$

where f_y is the yield stress and W_{el} the elastic section modulus. The squash load of the cross section was presented as follows:

$$N_{\text{pl}} = \left(1 + \rho\right) t_{\text{w}} h f_{\text{y}} = A f_{\text{y}} \tag{45}$$

where A is the area of the cross-section. The yield contour was given by two equations:

$$\begin{aligned} &\left|\frac{M}{M_{\text{y}}}\right| = 1.5\left(\lambda_3 - \lambda_2\left(\frac{N}{N_{\text{pl}}}\right)^2\right) \text{if} \left|\frac{N}{N_{\text{pl}}}\right| < \frac{1}{1+\rho} \\ &\left|\frac{M}{M_{\text{y}}}\right| = 3\lambda_1\left(1 - \left|\frac{N}{N_{\text{pl}}}\right|\right) \text{if} \left|\frac{N}{N_{\text{pl}}}\right| \geq \frac{1}{1+\rho} \end{aligned} \tag{46}$$

where:

$$\lambda_1 = (1 + \rho) / (1 + 3\rho) \tag{47}$$

$$\lambda_2 = (1 + \rho)^2 / (1 + 3\rho) \tag{48}$$

$$\lambda_3 = (1 + 2\rho) / (1 + 3\rho) \tag{49}$$

If ρ equals zero then the yield contour reduces to that of a rectangular cross-section with height h and width t_{w}. As ρ becomes larger the yield contour is that of a conventional wide flange section bent about its major axis. The yield contour of an open web section (wide flange section without a web) with a linear moment-normal force interaction is found when ρ equals infinity (Figure 12).

The yield contour by Yamasaki and Ishikawa (1968) is normalized with respect to the elastic moment capacity M_{y} instead of the plastic moment capacity M_{pl}. It can be seen that for a rectangular cross-section the plastic moment capacity is 1.5 times larger than the elastic moment capacity, i.e. the shape factor. The above yield contour is implemented in the iterative method for comparison with the results from Yamasaki and Ishikawa.

4.2. Comparison for Arches with a 120° Subtended Angle

Three-hinged arches with a fixed subtended angle but with different section height-to-span ratios (h/L) and ρ-values were analyzed by Yamasaki and Ishikawa (1968). Two loadcases were examined: a central point load and a uniformly distributed load. The plastic collapse load is normalized with respect to the squash load of the cross-section N_{pl} for the central load at the crown. For the uniformly distributed load, the plastic collapse load is non-dimensionalized with respect to the span length L and squash load. A full comparison of normalized collapse loads between the analyses of Yamasaki and Ishikawa (1968) and the authors is

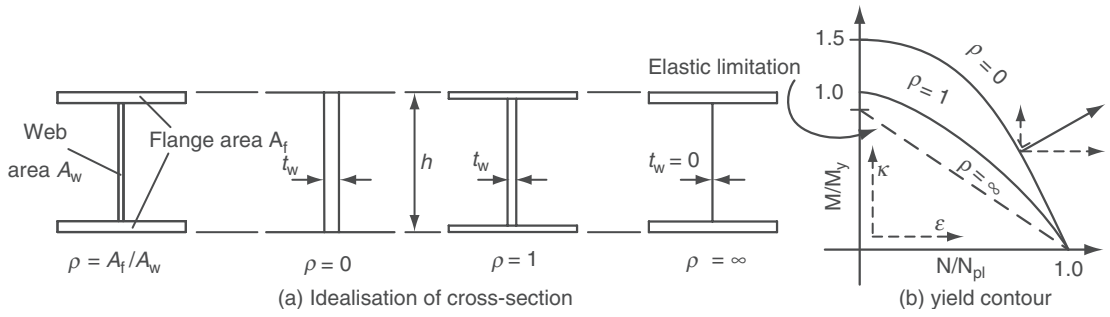

Figure 12. Idealization of cross-section by Yamasaki and Ishikawa (1968)

presented in Table 1 and Table 2 for an arch carrying a single force at the crown and a uniformly distributed load, respectively. A collapse load ratio is computed as F_{pl} (Yamasaki and Ishikawa (1968))/F_{pl} (Iterative method) for arches with a central point load. For arches with a uniformly distributed load the ratio is computed as q_{pl} (Yamasaki and Ishikawa (1968))/q_{pl} (Iterative method). In addition, the kinematic admissibility requirements are shown. It can be seen that the iterative method follows the results of Yamasaki and Ishikawa quite closely and that the deformation mode satisfies the kinematic admissibility requirements.

4.3. Comparison for Arches with other Subtended Angles

A similar comparison is made for three-hinged arches with identical load cases presented in section 4.2 but with other subtended angles. The h/L ratio and ρ-value are fixed at 0.05 and 0, respectively. From Table 3 it can be observed that the iterative method produces almost

Table 1. Comparison of normalized plastic collapse loads for three-hinged arches with central point load: subtended angle $2\gamma = 120°$

	$\rho = 0$					$\rho = 1$				
	Y.I*	Iterative method				Y.I*	Iterative method			
			Kinematic Admissibility					Kinematic Admissibility		
h/L	F_{pl}/N_{pl}	F_{pl}/N_{pl}	Δ_{ver}/φ_1	φ_2/φ_1	Ratio	F_{pl}/N_{pl}	F_{pl}/N_{pl}	Δ_{ver}/φ_1	φ_2/φ_1	Ratio
0.02	0.64	0.64	>0	>0	1.00	0.96	0.96	>0	>0	1.00
0.03	0.96	0.96	>0	>0	1.00	1.43	1.42	>0	>0	1.01
0.04	1.27	1.27	>0	>0	1.00	1.85	1.85	>0	>0	1.00
0.05	1.57	1.58	>0	>0	0.99	2.25	2.26	>0	>0	1.00

* Y.I. = Yamasaki and Ishikawa (1968)

Table 2. Comparison of normalized plastic collapse loads for three-hinged arches with uniformly distributed load: subtended angle $2\gamma = 120°$

	$\rho = 0$					$\rho = 1$				
	Y.I*	Iterative method				Y.I*	Iterative method			
			Kinematic Admissibility					Kinematic Admissibility		
h/L	$q_{pl}L/N_{pl}$	$q_{pl}L/N_{pl}$	Δ_{ver}/φ_1	φ_2/φ_1	Ratio	$q_{pl}L/N_{pl}$	$q_{pl}L/N_{pl}$	Δ_{ver}/φ_1	φ_2/φ_1	Ratio
0.02	4.46	4.48	>0	>0	1.00	6.05	6.03	>0	>0	1.00
0.03	6.23	6.26	>0	>0	1.00	7.80	7.85	>0	>0	0.99
0.04	7.65	7.70	>0	>0	0.99	9.05	9.11	>0	>0	0.99
0.05	8.80	8.86	>0	>0	0.99	10.0	10.1	>0	>0	0.99

* Y.I. = Yamasaki and Ishikawa (1968)

Table 3. Comparison of normalized plastic collapse loads for three-hinged arches with a central point load or uniformly distributed load: other subtended angles

	Central load					Uniformly distributed load				
		Iterative method					Iterative method			
	Y.I.*		Kinematic Admissibility			Y.I.*		Kinematic Admissibility		
γ[°]	F_{pl}/N_{pl}	F_{pl}/N_{pl}	Δ_{ver}/φ_1	φ_2/φ_1	Ratio	$q_{pl}L/N_{pl}$	$q_{pl}L/N_{pl}$	Δ_{ver}/φ_1	φ_2/φ_1	Ratio
10	0.113	0.114	>0	>0	0.99	0.345	0.346	>0	>0	1.00
20	0.155	0.156	>0	>0	0.99	0.660	0.666	>0	>0	0.99
30	0.169	0.170	>0	>0	0.99	0.905	0.914	>0	>0	0.99
40	0.170	0.171	>0	>0	0.99	1.030	1.041	>0	>0	0.99
50	0.165	0.166	>0	>0	0.99	1.013	1.022	>0	>0	1.01
60	0.157	0.158	>0	>0	0.99	0.880	0.886	>0	>0	0.99
70	0.146	0.147	>0	>0	0.99	0.698	0.702	>0	>0	0.99
80	0.133	0.134	>0	>0	0.99	0.525	0.528	>0	>0	0.99
90	0.119	0.120	>0	>0	0.99	0.383	0.385	>0	>0	0.99

* Y.I. = Yamasaki and Ishikawa (1968)

identical plastic collapse loads as found by Yamasaki and Ishikawa (1968).

4.4. Different Arch Configurations

Elastic-plastic analyses were conducted by Yamasaki and Ishikawa (1968) for a single arch geometry and cross-section, but with different arch configurations, i.e. support conditions, presence of crown-hinge. Three different arches were analyzed: three-hinged arch, pin-supported arch and fixed arch, the latter two without a crown-hinge. The accompanying load-deflection characteristics from elastic-plastic analyses by Yamasaki and Ishikawa are given in Figure 13 in addition to the plastic collapse loads obtained from the iterative method. The plastic collapse load F_{pl} is normalized with respect to the squash load N_{pl} of the cross-section. The plastic collapse analyses for the pin-supported arch and fixed arch were performed in conjunction with the iterative method as presented by Spoorenberg *et al*. (2012). It can be seen that the iterative method is able to replicate the plastic collapse load from the elastic-plastic computations with good accuracy.

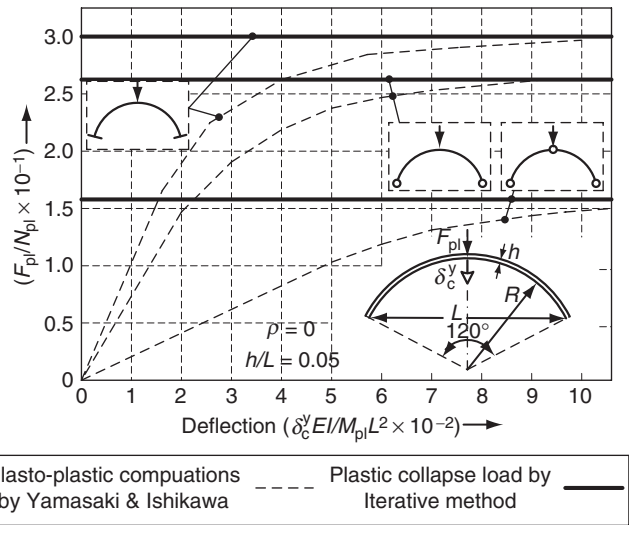

Figure 13. Load-deflection characteristic with results from iterative method (partly re-drawn from Yamasaki and Ishikawa 1968)

5. COMPARISON WITH FINITE ELEMENT RESULTS

5.1. Numerical Model

The plastic collapse loads from the iterative method are compared to results from finite element analyses. A finite element model was created in the ANSYS 11.0 environment: ANSYS guide (2009). The arch-rib was modeled with shell elements of the type SHELL181. Based on an earlier mesh refinement investigation, Spoorenberg *et al*. (2012), the arch was meshed with 8 elements over the width of the flanges, 8 elements over the height of the web and 96 elements along the developed length, comprising a total of 2304 shell elements. A HE 300A section was modeled. As the wide flange section is composed of three plated elements modeled with shells, the fillets are omitted. An asterisk * is introduced to make a distinction between the modeled section without fillets and the commercially available steel section. A bi-linear material model with yield stress f_y = 235 N/mm^2 and Young's modulus E = 200 000 N/mm^2 was employed to define the material response under loading. The width of the flange is b = 300 mm, the section height

h = 290 mm, the flange thickness t_f = 14 mm and the web thickness t_w = 8.5 mm.

5.1.1. Hinge modeling

The arch was modeled with two separate curvilinear sections jointed at the crown (Figure 14). The hinge at the crown was modeled by a set of coupled degrees of freedom [Figure 15(a)]. In order to avoid high stress concentrations MPC184 elements were applied over the cross-section on both sides of the hinge. The translations in all three directions and rotations about the x-axis and z-axis of the mid-height node of the left section were coupled to the equivalent node on the right side. Only the rotations about the y-axis were not coupled, allowing the desired hinge behavior during loading to occur [Figure 15(b)]. It can be seen that contact between the upper flanges of the two curvilinear segments is not modeled and the elements move 'through' each other.

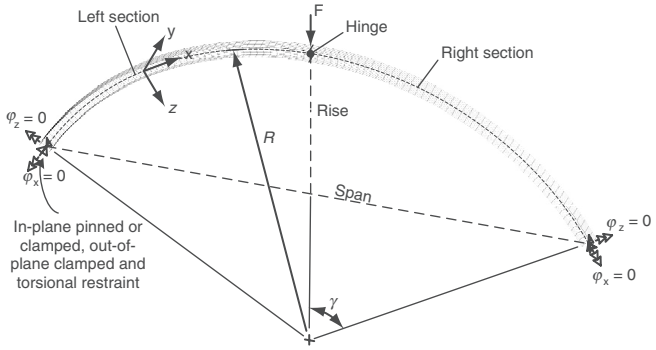

Figure 14. Finite element model of three-hinged arch with central point load at the crown

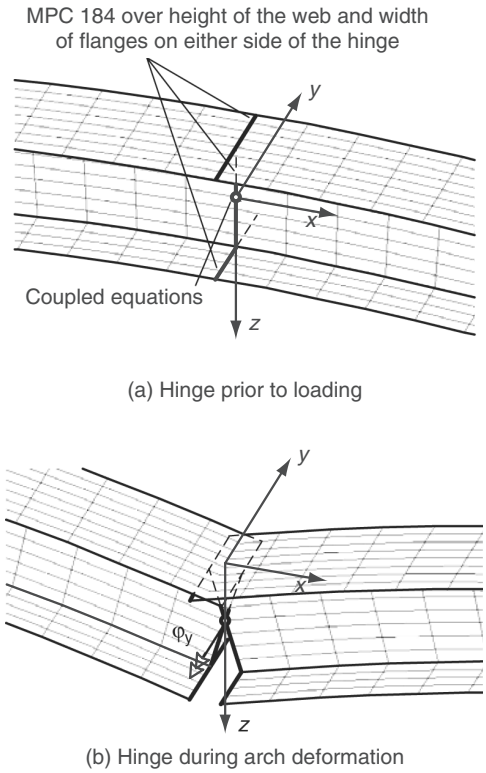

Figure 15. Crown hinge rotation

5.1.2. Loading and boundary conditions

At the supports the arches were constrained against translation in all three directions and rotations with respect to the z-axis and x-axis (Figure 14). For one-hinged arches, rotations at the support about the y-axis were constrained as well. Multipoint constraint elements were applied over the cross-section at the support in order to avoid high stress concentrations (Figure 16). Identical elements (MPC184) and element distribution as applied at the crown hinge were applied at the support. Loads were applied at the mid-height of the cross-section. The uniformly distributed load was applied in the numerical model by means of vertical point loads acting over the arch-rib.

5.1.3. Solution procedure and post-processing

A first order analysis was performed, taking into account material non-linearities, but ignoring the influence of deformations on the equilibrium equations. The Newton-Raphson method was selected to solve the non-linear equilibrium equations. All analyses were load-controlled. Equilibrium equations were considered solved when the out-of-balance load vector is less than 0.05% of the applied loading and when the out-of-balance displacement increment vector is smaller than 0.05% of the displacement increments. The load-deflection characteristics from the elastic-plastic computations are presented in Figure 17 for a HE 300A* arch with a developed

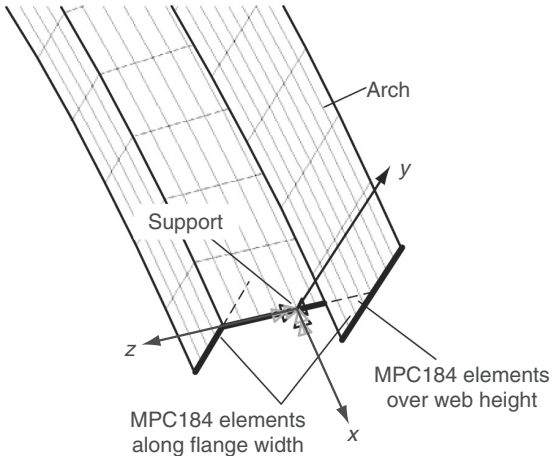

Figure 16. Detail of support

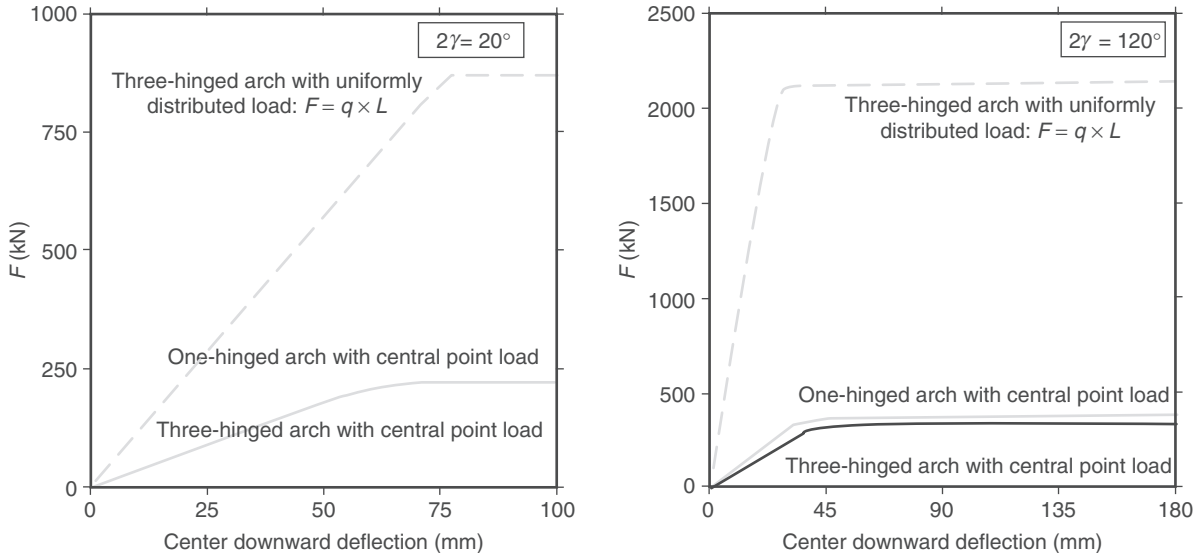

Figure 17. Load-deflection characteristics for HE 300A*, S = 12 m

length of 12 m and two different subtended angles: $2\gamma = 20°$ and $2\gamma = 120°$. The uniformly distributed load is multiplied by the arch span L in order to display the load-deflection characteristics in the same graph with the other load cases. The load level at which further increase in load results in virtually unbounded deflections is identified as the plastic collapse load. The equivalent plastic strain distributions at plastic collapse is shown in Figure 18 for one-hinged arches with $2\gamma = 120°$ and $2\gamma = 20°$. From this representation it can be seen that four plastic hinges and two plastic hinges are formed in the arch rib when a flexural

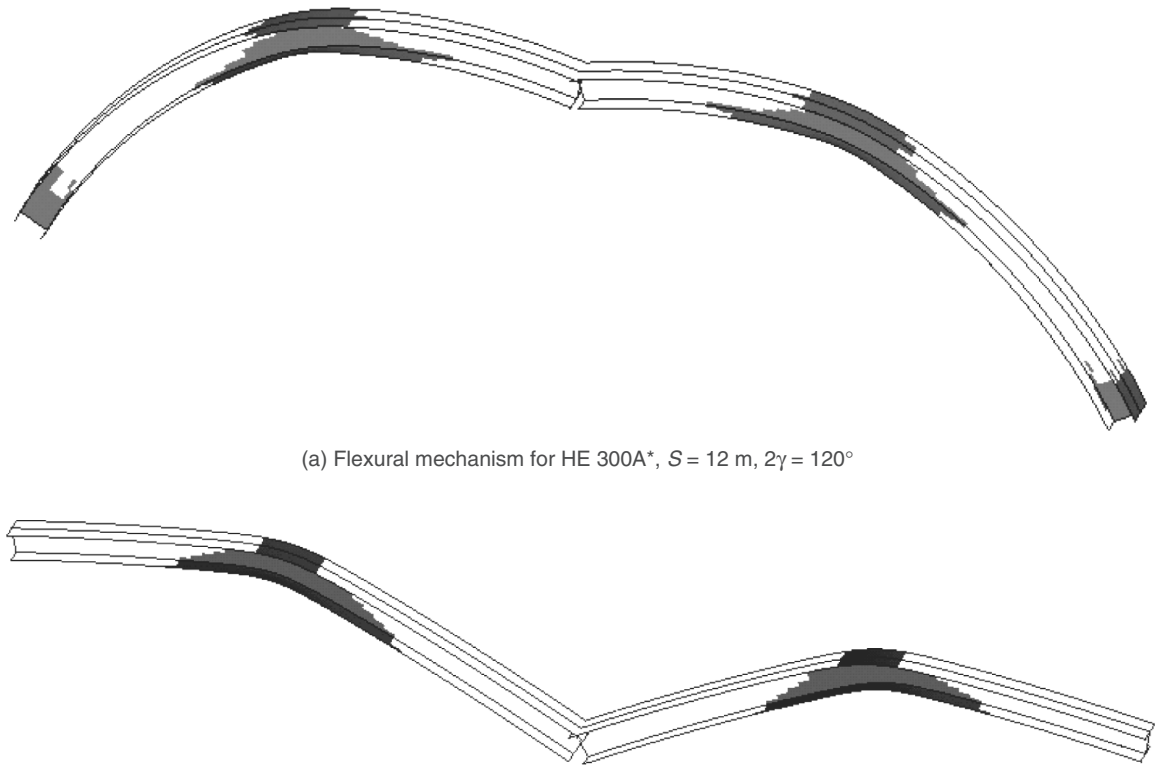

(a) Flexural mechanism for HE 300A*, S = 12 m, $2\gamma = 120°$

(b) Compressive mechanism for HE 300A*, S = 12 m, $2\gamma = 20°$

Figure 18. Equivalent plastic strains at failure (mesh not shown for clarity) for a one-hinged arch

mechanism or a compressive mechanism take place, respectively.

5.2. Three-Hinged Arch with Central Point Load

A full comparison between the results from non-linear finite element analyses and the iterative method is presented in Table 4. HE 300A* arches with a developed arch length S = 12 m and S = 16 m were selected for a comparative study. It can be seen that the iterative method is able to replicate the results of the elastic-plastic computations with good accuracy. The ratio is evaluated as: F_{pl} (ANSYS)/F_{pl} (Iterative method). The kinematic admissibility requirements are met for all investigated arches.

5.3. Three-Hinged Arch with Uniformly Distributed Load

The same group of arches is selected to assess the performance of the iterative method for a uniformly distributed load. The comparison between the plastic collapse load from elastic-plastic computations with the finite element method and the iterative method is presented in Table 5. It can be seen that the iterative method produces good approximations of the finite element results. The iterative method meets the kinematical requirements for all investigated arches.

5.4. One-Hinged Arch with Central Point Load

A comparison between the plastic collapse load obtained from the iterative method and finite element computation with ANSYS are shown in Table 6 for one-hinged arches with a central point load. It can be seen that even for a number of arches for which one kinematic admissibility requirement is not met, the iterative method produces reasonably accurate values of the plastic collapse load. In these cases the arches are shallow and a compressive mechanism is determining the arch behavior, Figure 18(b).

Table 4. Comparison of plastic collapse loads (kN) of three-hinged HE 300A* arches with central point load

	S = 12 m					S = 16 m				
	ANSYS	Iterative method				ANSYS	Iterative method			
			Kinematic Admissibility					Kinematic Admissibility		
2γ[°]	F_{pl}	F_{pl}	Δ_{ver}/φ_1	φ_2/φ_1	Ratio	F_{pl}	F_{pl}	Δ_{ver}/φ_1	φ_2/φ_1	Ratio
10	151	150	>0	>0	1.01	139	136	>0	>0	1.02
30	272	278	>0	>0	0.98	229	234	>0	>0	0.98
60	347	352	>0	>0	0.99	274	283	>0	>0	0.97
90	371	384	>0	>0	0.97	291	303	>0	>0	0.96
120	377	399	>0	>0	0.94	294	302	>0	>0	0.97
150	371	397	>0	>0	0.93	291	298	>0	>0	0.98
180	375	391	>0	>0	0.96	287	293	>0	>0	0.98

Table 5. Comparison of plastic collapse loads (kN/m) of three-hinged HE 300A* arches with uniformly distributed load

	S = 12 m					S = 16 m				
	ANSYS	Iterative method				ANSYS	Iterative method			
			Kinematic Admissibility					Kinematic Admissibility		
2γ[°]	q_{pl}	q_{pl}	Δ_{ver}/φ_1	φ_2/φ_1	Ratio	q_{pl}	q_{pl}	Δ_{ver}/φ_1	φ_2/φ_1	Ratio
10	36.3	36.3	>0	>0	1.00	27.2	27.2	>0	>0	1.00
30	107	107	>0	>0	1.00	79.5	79.3	>0	>0	1.00
60	188	185	>0	>0	1.02	132	132	>0	>0	1.00
90	214	209	>0	>0	1.02	144	140	>0	>0	1.03
120	201	196	>0	>0	1.03	130	124	>0	>0	1.05
150	173	173	>0	>0	1.00	106	106	>0	>0	1.00
180	153	153	>0	>0	1.00	89	91.5	>0	>0	0.97

Table 6. Comparison of plastic collapse loads (kN) of one-hinged HE 300A* arches with central point load

	S = 12 m						S = 16 m					
		Iterative method						Iterative method				
	ANSYS		Kinematic Admissibility				ANSYS		Kinematic Admissibility			
2γ[°]	F_{pl}	F_{pl}	Δ_{ver}/φ_1	φ_2/φ_1	φ_3/φ_1	Ratio	F_{pl}	F_{pl}	Δ_{ver}/φ_1	φ_2/φ_1	φ_3/φ_1	Ratio
10	163	138	>0	>0	**<0**	1.18	141	128	>0	>0	**<0**	1.10
30	284	281	>0	>0	**<0**	1.01	259	243	>0	>0	>0	1.07
60	380	379	>0	>0	>0	1.00	316	312	>0	>0	>0	1.01
90	430	428	>0	>0	>0	1.00	346	344	>0	>0	>0	1.01
120	449	456	>0	>0	>0	0.98	355	361	>0	>0	>0	0.98
150	454	473	>0	>0	>0	0.96	360	367	>0	>0	>0	0.98
180	467	481	>0	>0	>0	0.97	366	364	>0	>0	>0	1.01

6. DESIGN GRAPHS

The results of the iterative method are collated and converted into design graphs to allow a quick estimate of the plastic collapse load of crown-hinged arches. A non-dimensional slenderness parameter λ is used to allow design graphs for a broad range of arch geometries to be developed.

$$\lambda = \frac{M_{pl}}{N_{pl}S} \tag{50}$$

This non-dimensional parameter has been introduced earlier by Chakrabarty (1988) and Maeda and Fujimoto (1970) to present the plastic collapse load of steel arches to be independent of the arch geometry. The plastic collapse load will be presented in non-dimensional form:

$$w_F = \frac{F_{pl}R}{M_{pl}} \tag{51}$$

$$w_Q = \frac{q_{pl}R^2}{M_{pl}} \tag{52}$$

where w_F and w_Q are the normalized plastic collapse loads for an arch with a central point load and with a uniformly distributed load, respectively.

Design graphs were developed for two different yield contours: the yield contour presented in section 2.3 in addition to a contour given in Eurocode 3, EN 1993-1-1 (2004). According to Eurocode 3 no allowance for the influence of normal force has to be made if the following requirements are met:

$$|N| \le 0.25N_{pl} \text{ and } |N| \le 0.5h_0 t_w f_y / \gamma_{M0} \tag{53}$$

In case the requirements from Eqn 53 are violated the plastic moment capacity needs to be reduced according to the following yield contour ψ:

$$\psi = \left|\frac{M}{M_{pl}}\right| \le \left(1 - \left|\frac{N}{N_{pl}}\right|\right) \Big/ (1 - 0.5a)$$
$$a = \left(A - bt_f\right)/A \tag{54}$$

where:

h_0 is the height of the web (or $h - 2t_f$)

γ_{M0} is the partial factor for cross-section resistance, recommended value: 1.0

The normalized plastic collapse load is plotted for various λ-values in Figure 19, Figure 20 and Figure 21 for three-hinged arches with a central point load, three-hinged arches with a uniformly distributed load and one-hinged arches with a central point load using the yield contour of 2.3 and the yield contour according to Eurocode 3. The subtended angle is varied between 10 and 180 degrees.

The kinematic admissibility requirement imposes a restriction on the applicability of the iterative method for one-hinged arches. For arches with relatively small subtended angles the kinematic admissibility requirements are not met since a compressive mechanism is present and the obtained results cannot be used. The subtended angles of arches for which the kinematic admissibility requirements are not met are a function of the non-dimensional slenderness λ. For arches with relatively high λ-values the threshold angle beyond which the iterative method can be used is 50 degrees. For arches with small λ-values this threshold angle is 20 degrees. The solid

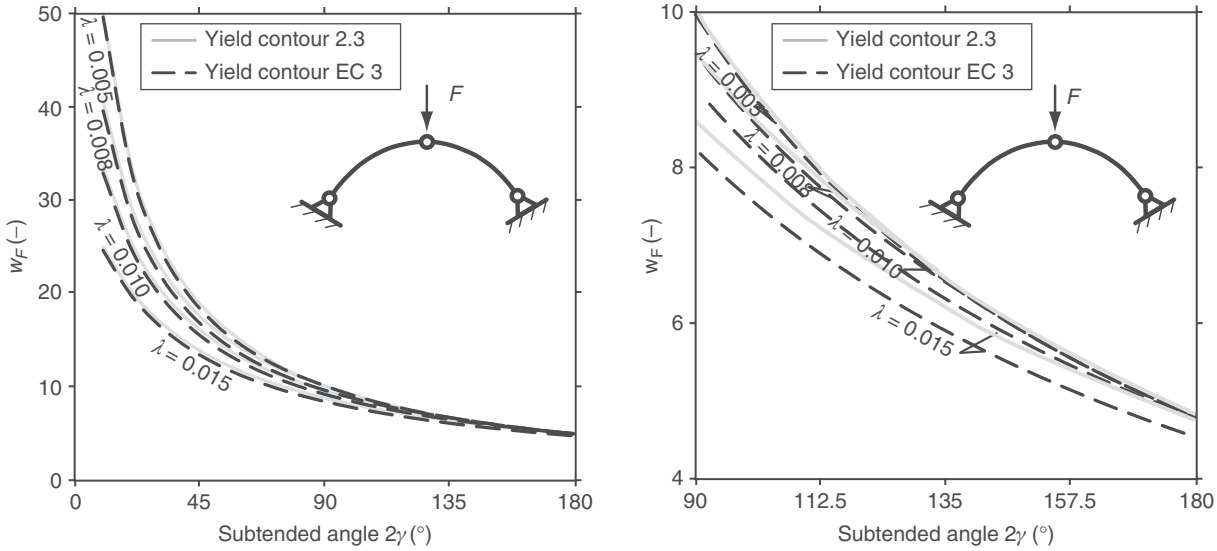

Figure 19. Normalized collapse load w_F for three-hinged arch with central point load (enlarged scales on the right)

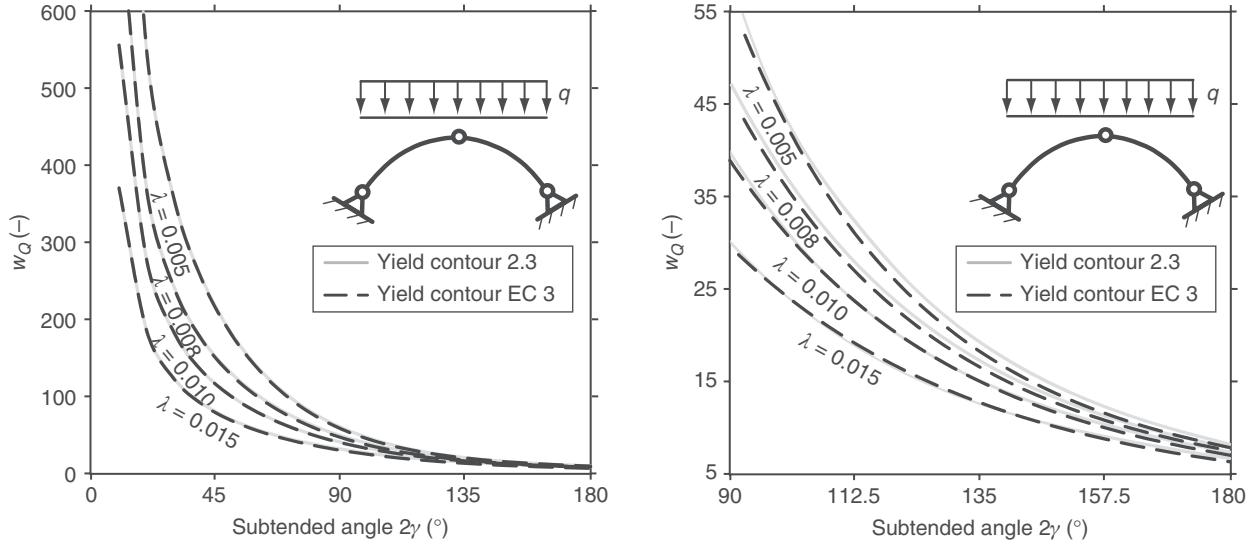

Figure 20. Normalized collapse load w_Q for three-hinged arch with uniformly distributed load (enlarged scales on the right)

black curve in Figure 21 illustrates the applicability of the iterative method: the kinematic admissibility requirements are met for one-hinged arches with subtended angles 2γ and non-dimensional slenderness values to the right of the solid black curve.

Figure 19, Figure 20 and Figure 21 clearly show that for a specific subtended angle increasing the value of λ will decrease the normalized collapse load. For a constant value of λ the normalized collapse load increases as the subtended angle decreases. These trends are observed consistently in all design graphs. For the HE 300A* section the choice for the yield contour has a minor influence on the plastic collapse load. Using the yield contour of Eurocode 3 yields lower plastic collapse loads compared to the yield contour of section 2.3.

7. INFLUENCE OF CROWN-HINGE

The influence of a crown hinge introduction on the plastic collapse load can be shown by presenting the ratio of the collapse loads of equivalent arches with and without a crown hinge as a function of λ and the subtended angle. The results are obtained for two different yield contours: according to section 2.3 and according to Eurocode 3. When the kinematic admissibility requirements are violated the curves are dotted as shown in the previous section. The data from arches without crown hinges are obtained from Spoorenberg *et al*. (2012).

7.1. Three-Hinged Arch with Central Point Load

The plastic collapse load for three-hinged arches with a central point load is normalized with respect to the

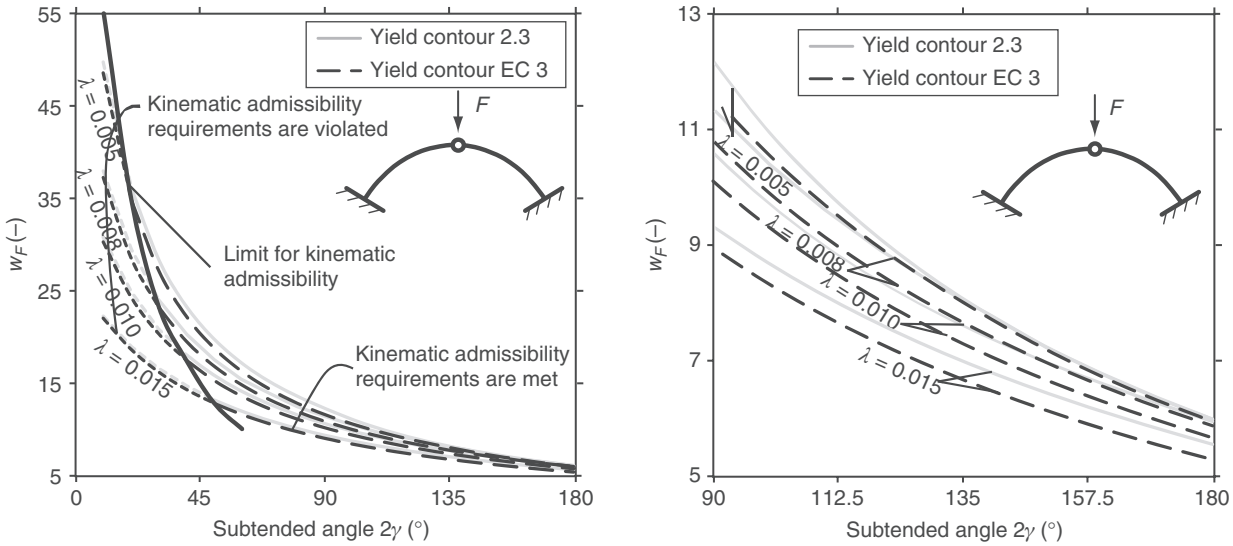

Figure 21. Normalized collapse load w_F for one-hinged arch with central point load (enlarged scales on the right)

plastic collapse load obtained from equivalent arches without a crown hinge. The latter group is denoted as two-hinged. Two hinged arches are also known as pin-supported arches. The collapse loads of three-hinged arches and two-hinged arches are abbreviated with "3 h" and "2 h", respectively, as shown in Figure 22. It is clearly visible that the influence of introducing a hinge at the crown is most detrimental to arches with large subtended angles and small λ values. The plastic collapse load for a three-hinged arch is approximately 60% of the plastic collapse load of its pin-supported counterpart when the subtended angle is 180°. It can be seen that the curves generally show a gradual decrease in percentages with increasing subtended angle. The gradual change in percentage is disturbed for arches with $\lambda = 0.005$ and $\lambda = 0.008$ and $70 \leq 2\gamma \leq 180$. This is the result of the employment of bi-linear yield contours.

7.2. Three-Hinged Arch with Uniformly Distributed Load

The same comparison as for arches with a central load at the crown is made for arches subjected to a uniformly distributed load. The plastic collapse load for a three-hinged arch is normalized with respect to the plastic collapse load of its pin-supported equivalent. The plastic collapse loads of the latter group are obtained from Spoorenberg *et al.* (2012). The results are shown in Figure 23. It can be seen that

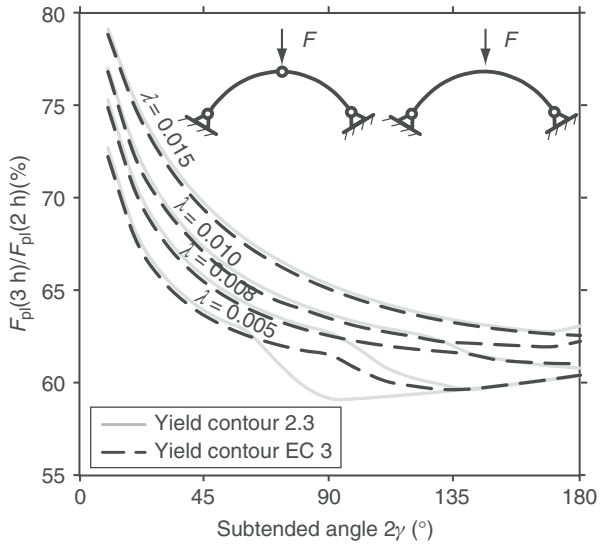

Figure 22. Ratio of central point loads for plastic collapse of three-hinged arches and two-hinged arches

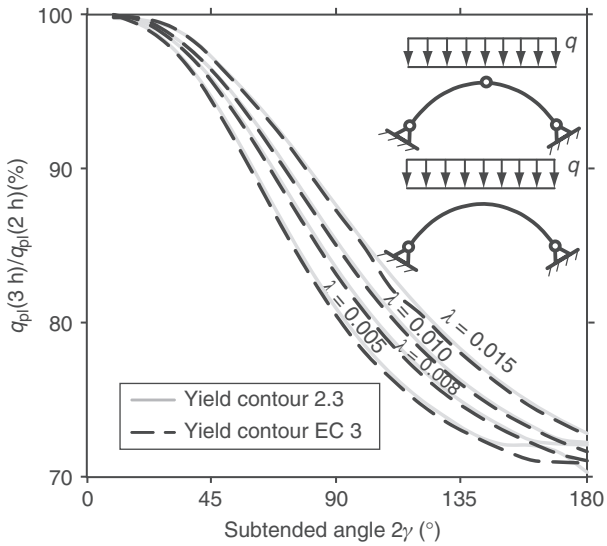

Figure 23. Ratio of uniformly distributed loads for plastic collapse of three-hinged arches and two-hinged arches

the effect of introducing a hinge at the crown for an arch under a uniformly distributed load is most profound for arches with relatively large subtended angles and small λ-values. For semi-circular arches the introduction of a hinge at the crown can result in a decrease in plastic collapse load of approximately 30%. When comparing Figure 22 with Figure 23 it can be seen that introducing a hinge at the crown in a pin-supported arch with a central point load is more detrimental to the normalized plastic collapse load than for the same arches with a uniformly distributed load. This is partly attributed to the phenomenon that the presence of a hinge at the crown is more detrimental for arches subject to predominantly bending actions, such as arches with a central point load.

7.3. One-Hinged Arch with Central Point Load

Similarly to one hinged arches, the kinematic admissibility for fixed or zero-hinged arches restricts the applicability of the iterative method to non-shallow arches. A comparison is made between one-hinged arches and their zero-hinged equivalents where the kinematic admissibility requirements are met for both arches. The one-hinged arch is denoted as "1 h" and the zero-hinged arch is denoted as "0 h". In Figure 24 the plastic collapse load for one-hinged arches is normalized with respect to the plastic collapse load from its zero-hinged equivalent. It can be seen that the reduction in plastic collapse load due to the presence of a crown hinge is most significant for arches with large subtended angles and small λ values.

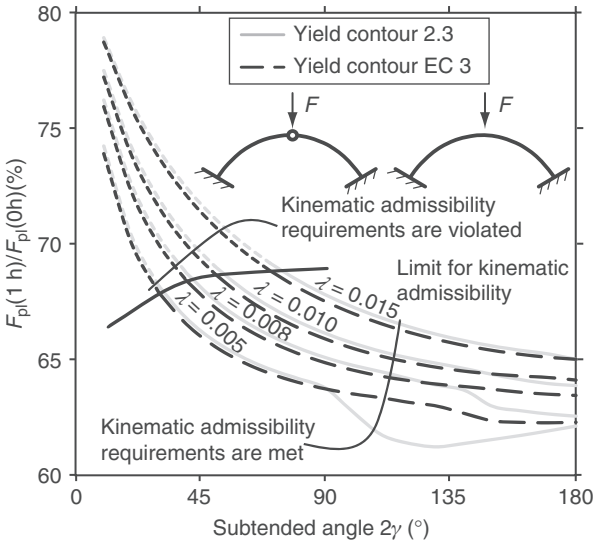

Figure 24. Ratio of central point loads for plastic collapse of one-hinged arches and zero-hinged arches

8. DISCUSSION

8.1. Change of Mechanism

From the preceding sections it was found that the iterative method produces accurate values of the plastic collapse load for three-hinged arches with a central point load, three-hinged arches with a uniformly distributed load and one-hinged arches with a central point load. For shallow one-hinged arches it was found that the iterative method produces less accurate results, which is attributed to an incorrect assumption of the collapse mechanism as illustrated by the violation of the kinematic admissibility requirements. Shallow one-hinged arches fail by a compressive mechanism while for the iterative method a flexural mechanism is assumed. The threshold angle 2γ beyond which the adopted collapse mechanism meets the kinematic admissibility requirements depends in one-hinged arches on the arch slenderness λ which varies between 20 and 50 degrees.

8.2. Use of Different Yield Contours

In the theoretical analyses three different yield contours for a wide flange section bent about the major axis were used: Eqn 1, Eqn 46 and Eqn 54. The iterative method allows the use of different yield contours without re-deriving the equilibrium equations by simply replacing the description of the yield contour. The suggested method can be used for wide flange sections subject major axis bending and compression for which yield contours are provided by others, e.g. Chen and Atsuta (1977), Horne (1979), Orbison *et al.* (1982) and Duan and Chen (1990).

The iterative method is also applicable to wide flange sections bent about their minor axis which have a significantly different yield contour from wide flange sections bent about their major axis. Asymmetric yield contours such as proposed by Kitipornchai *et al.* (1991) can also be used in the presented method to find the plastic collapse load of arches made from T-, L- or monosymmetric I-sections. In these cases a distinction must be made between the yield contours for hogging moments and sagging moments.

9. CONCLUSIONS

This paper presented an analytical approach to obtain the plastic collapse load for three-hinged arches with a central point load, three-hinged arches with a uniformly distributed load and one-hinged arches with a central point load. Three-hinged arches are pin-supported arches with a hinge at the crown and one-hinged arches are fixed arches with a hinge at the crown. The lower bound theorem, upper bound theorem and kinematic admissibility requirements as part of plastic theory were

used for the analyses. The reduction of the plastic moment capacity by normal force was taken into account. Due to the presence of a non-linear relationship between the acting loads and the reduction in plastic moment capacity, it was found necessary to employ iterative techniques to arrive at the plastic collapse load.

All analyses were limited to steel circular arches made from wide flange sections bent about their major axis. Earlier studies and finite element analyses were selected for a comparative study from which it was concluded that the iterative method is able to approximate the plastic collapse load with good accuracy.

Design graphs were developed containing plastic collapse loads obtained with the iterative method for a wide range of arch geometries, enabling a quick estimate of the plastic collapse load without taking recourse to the iterative method or finite element analysis. The design graphs were derived independently of the arch geometry through the introduction of a single arch slenderness parameter, allowing the plastic collapse loads to be presented in non-dimensional form.

Plastic collapse loads of crown-hinged arches were expressed as a percentage of the plastic collapse load for equivalent arches without a crown hinge to show the net influence of the introduction of a hinge at the crown. It was found that the magnitude of the decrease in plastic collapse load by introducing a crown hinge depends on the type of loading, support conditions and arch geometry. For arches featured by predominantly compressive action in the arch-rib, such as shallow arches and arches with a uniformly distributed load, the introduction of a crown hinge will result in only a small reduction of the plastic collapse load. A larger decrease was observed for deep arches with a central point load and predominant bending action in the arch-rib.

The presented iterative method can be applied to crown-hinged arches with different yield contours and geometries.

REFERENCES

ANSYS (2009). *ANSYS Structural Analysis Guide*, Release 11.0, ANSYS Inc., Canonsburg, PA, USA.

Bakker, M.C.M., Spoorenberg, R.C., Snijder, H.H. and Hoenderkamp, J.C.D. (2008). "In-plane plastic limit load of steel circular arches, a lower bound limit analysis approach", *Proceedings of the 5th European Conference on Steel and Composite Structures (Eurosteel)*, Graz, Austria, pp. 1831–1836.

Chakrabarty, J. (1988). *Theory of Plasticity*, McGraw-Hill, London, UK.

Chen, W.F. and Atsuta, T. (1977). *Theory of Beam-Columns*, *Vol.2*, *Space Behavior and Design*, McGraw-Hill, New York, USA.

Duan, L. and Chen, W.F. (1990). "A yield surface equation for doubly symmetrical sections", *Engineering Structures*, Vol. 12, No. 2, pp. 114–119.

EN 1993-1-1 (2004). *Eurocode 3. Design of Steel Structures*, *General Rules and Rules for Buildings*, CEN European Committee for Standardization, Brussels, Belgium.

Hayashi, T. (1971). *Handbook of Structural Stability*, Corona Publishing Company, Ltd., Tokyo, Japan.

Horne, M.R. (1979). *Plastic Theory of Structures*, Pergamon press, Oxford, UK.

Kitipornchai, S., Zhu, K., Xiang, Y. and Al-Bermani, F.G.A. (1991). "Single-equation yield surfaces for monosymmetric and asymmetric sections", *Engineering Structures*, Vol. 13, No. 4, pp. 366–370.

Maeda, Y. and Fujimoto, K. (1970). "Study on calculation of plastic collapse load of two-hinged arch", *Transactions of the Japan Society of Civil Engineers*, Vol. 174, No. 2, pp. 25–40.

Orbison, J.G., McGuire, W. and Abel, J.F. (1982). "Yield surface applications in nonlinear steel frame analysis", *Computer Methods in Applied Mechanics and Engineering*, Vol. 33, No. 1–3, pp. 557–573.

Spoorenberg, R.C., Snijder, H.H. and Hoenderkamp, J.C.D. (2012). "A theoretical method for calculating the collapse load of steel circular arches", *Engineering Structures*, Vol. 38, pp. 89–103.

Timoshenko, S.P. and Gere, J.M. (1961). *Theory of Elastic Stability*, McGraw-Hill, Tokyo, Japan.

Trahair, N.S., Bradford, M.A., Nethercot, D.A. and Gardner, L. (2007). *The Behaviour and Design of Steel Structures to EC3*, 4th edition, Taylor & Francis Group, London, UK.

Trahair, N.S., Pi, Y.L., Clarke, M.J. and Papangelis, J.P. (1997). "Plastic design of steel arches", *Advances in Structural Engineering*, Vol. 1, No. 1, pp. 1–9.

Yamasaki, T. and Ishikawa, N. (1968). "Elasto-plastic analysis of circular arches", *Transactions of the Japan Society of Civil Engineers*, Vol. 158, No. 10, pp. 1–16.